Progression of vascular remodeling in pulmonary vein obstruction

Check for updates

Naoki Masaki, MD, PhD,[a] Osamu Adachi, MD, PhD,[a] Shintaro Katahira, MD, PhD,[a] Yuriko Saiki, MD, PhD,[b] Akira Horii, MD, PhD,[b] Shunsuke Kawamoto, MD, PhD,[a] and Yoshikatsu Saiki, MD, PhD[a]

ABSTRACT

Objectives: Pulmonary vein obstruction (PVO) frequently occurs after repair of total anomalous pulmonary vein connection with progression of intimal hyperplasia from the anastomotic site toward upstream pulmonary veins (PVs). However, the understanding of mechanism in PVO progression is constrained by lack of data derived from a physiological model of the disease, and no prophylaxis has been established. We developed a new PVO animal model, investigated the mechanisms of PVO progression, and examined a new prophylactic strategy.

Methods: We developed a chronic PVO model using infant domestic pigs by cutting and resuturing the left lower PV followed by weekly hemodynamic parameter measurement and angiographic assessment of the anastomosed PV. Subsequently, we tested a novel therapeutic strategy with external application of rapamycin-eluting film to the anastomotic site.

Results: We found the pig PVO model mimicked human PVO hemodynamically and histopathologically. This model exhibited increased expression levels of Ki-67 and phospho-mammalian target of rapamycin in smooth muscle-like cells at the anastomotic neointima. In addition, contractile to synthetic phenotypic transition; that is, dedifferentiation of smooth muscle cells and mammalian target of rapamycin pathway activation in the neointima of upstream PVs were observed. Rapamycin-eluting films externally applied around the anastomotic site inhibited the activation of mammalian target of rapamycin in the smooth muscle-like cells of neointima, and delayed PV anastomotic stenosis.

Conclusions: We demonstrate the evidence on dedifferentiation of smooth muscle-like cells and mammalian target of rapamycin pathway activation in the pathogenesis of PVO progression. Delivery of rapamycin to the anastomotic site from the external side delayed PV anastomotic stenosis, implicating a new therapeutic strategy to prevent PVO progression. (J Thorac Cardiovasc Surg 2020;160:777-90)

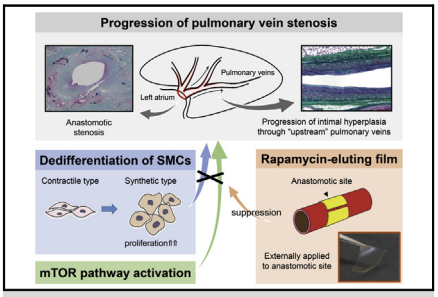

Pathogenesis of PVO progression and a possible therapeutic option for prevention of PVO.

CENTRAL MESSAGE

SMC-like cells dedifferentiation and mTOR pathway activation may be involved in progression of PVO. Externally applied rapamycin-eluting films can transiently suppress PVO progression.

PERSPECTIVE

Dedifferentiation of SMC-like cells and mTOR pathway activation appeared to be involved in the pathogenesis of PVO progression. Local delivery of rapamycin to the anastomotic site from the external side delayed PV anastomotic stenosis implicating a new therapeutic strategy to prevent PVO progression.

See Commentaries on pages 791, 792, and 794 .

Surgical outcome of total anomalous pulmonary vein connection (TAPVC) repair has progressively improved; however, pulmonary vein obstruction (PVO) remains a serious postoperative complication after TAPVC repair.[1-3] Although treatments for PVO include surgical intervention,[4,5] and endovascular therapy,[6] the risk of recurrence is still quite high and patients experiencing posttreatment PVO have poor prognosis.[4,5,7,8] Fibrosis and intimal hyperplasia at the anastomotic site and

From the [a]Division of Cardiovascular Surgery and [b]Department of Molecular Pathology, Tohoku University Graduate School of Medicine, Aoba-ku, Sendai, Japan.

Supported by the Japan Society for the Promotion of Science (JSPS) KAKENHI grant No. 24592047.

Received for publication Jan 16, 2019; revisions received Dec 24, 2019; accepted for publication Jan 20, 2020; available ahead of print Feb 26, 2020.

Address for reprints: Yoshikatsu Saiki, MD, PhD, Division of Cardiovascular Surgery, Tohoku University Graduate School of Medicine, 1-1 Seiryomachi, Aoba-ku, Sendai 980-8574, Japan (E-mail: yoshisaiki@med.tohoku.ac.jp).

0022-5223/$36.00

Copyright © 2020 by The American Association for Thoracic Surgery

https://doi.org/10.1016/j.jtcvs.2020.01.098

Scanning this QR code will take you to the article title page to access supplementary information.

Abbreviations and Acronyms

4E-BP1 = eukaryotic translation initiation factor 4E-binding protein 1
αSMA = alpha-smooth muscle actin
H-RAP = high-dose rapamycin film
L-RAP = low-dose rapamycin film
mTOR = mammalian target of rapamycin
PAP = pulmonary arterial blood pressure
PCWP = pulmonary capillary wedge pressure
PV = pulmonary vein
PVO = pulmonary vein obstruction
SMC = smooth muscle cell
SMemb = non-muscle myosin heavy chain
TAPVC = total anomalous pulmonary vein connection
TGF-β1 = transforming growth factor-beta1

progression of intimal lesions toward the upstream pulmonary veins (PVs) in the lung parenchyma are reported to be the main histopathologic changes in PVO.[1,3,5,9] However, the mechanisms by which intimal lesions diffusely progress to upstream PVs remain unknown.

LaBourene and colleagues[10] established a porcine PVO model by performing PV banding,[10] and this model has been studied to clarify the mechanisms of PVO progression.[9,11] However, it does not employ a clinically relevant anastomotic site, and typical histopathologic changes developing at the origin of the vasculopathy were not observed. Therefore, a new model mimicking surgical treatment is needed for further understanding of PVO.

The aims of this study are to establish a new PVO animal model using PV cut-and-suture technique, to elucidate the histopathologic changes at the anastomosed site, and to reveal the mechanism underlying PVO progression toward upstream PVs. Furthermore, we also examined the effectiveness of externally applied rapamycin-eluting films as a prophylaxis of PVO progression.

MATERIALS AND METHODS

Detailed methods are provided in Appendix E1. All animal experiments were approved by the Tohoku University (Sendai, Japan) Animal Care and Use Committee (No. 2013-416 and No. 2015-035).

Animal

Domesticated pigs aged 6 to 8 weeks weighing 17.9 ± 2.1 kg were used in these experiments.

Surgical Procedure

Pigs were placed in the right decubitus position, and a left fifth intercostal thoracotomy was performed. The left pulmonary artery was selectively occluded using a Swan-Ganz catheter and the left lower PV clamped. The PV was transected near-circumferentially leaving a 2- to 3-mm bridge of posterior wall, and the edges were re-anastomosed with a running 7–0 Prolene (Ethicon, Somerville, NJ) suture, including undivided posterior wall (Figure 1, *A* and *B*) (PVO: 1 week model; n = 5, and 8 weeks model; n = 7). A natural purse string stricture at the anastomotic site was encountered, and postoperative diameter of the left lower PV was approximately 70% of preoperative diameter (Table E1). The sham group (1 week model; n = 5, and 8 weeks model; n = 4) underwent identical procedures, including clamp of the left lower PV for 20 to 25 minutes, with the exception of cut and suture of the PV. We evaluated model validity in Experiment I and the effectiveness of rapamycin film treatment in Experiment II. An overview of the protocols is shown in Figure 2.

Preparation of Rapamycin-eluting Film and Treatment

Rapamycin-eluting films were prepared as described in our previous study.[12] The films were 45.2 ± 10.0 μm thick (Figure E1, *A* and *B*). In vitro cumulative release of rapamycin from the film was approximately 15% after 1 week, 30% after 2 weeks, and 75% after 4 weeks (Figure E2, *A*). Additionally, estimated in vivo rapamycin release was approximately 40% after 1 week, 70% after 2 weeks, and 100% after 4 weeks (Figure E2, *B*).

Another 15 pigs were allocated to the rapamycin film treatment study (Figure 2). We tested both a low-dose film containing 1 mg rapamycin (L-RAP) (8 weeks model; n = 5) and a high-dose film containing 10 mg (H-RAP) (1 week model; n = 5, and 8 weeks model; n = 5). An identical application protocol was used for both, which involved encircling the anastomotic site as shown in Figure E1, *C*.

Hemodynamic Assessment and Angiography

Hemodynamic assessment and pulmonary arterial angiography for the evaluation of anastomosed PV patency were performed weekly after surgery. These were continued until the anastomosed PV was found to be occluded by digital subtraction angiography.

Histologic Analysis

Pulmonary vein tissue from the anastomotic site to the most distal retrievable upstream site was divided into 3 segments (Figure E3) for histologic analysis (Sham 8 weeks model; n = 4, and the others; n = 5). Paraffin-embedded tissues were sectioned and stained with hematoxylin and eosin. Elastica-Masson staining was performed to quantify intimal hyperplasia and intima-media hypertrophy in each segment. Results are expressed as area normalized to local vessel caliber (area/radius^2).

Immunohistochemistry

Other sections were labeled with antibodies against CD31, alpha-smooth muscle actin (αSMA), nonmuscle myosin heavy chain (SMemb), h-caldesmon, calponin, Ki-67, and phospho-mammalian target of rapamycin (p-mTOR) (Ser2448) (n = 5 in each group). The Ki-67-positive and p-mTOR-positive cells in the neointimal area were counted in 5 different fields (40× objective) using the color deconvolution plug-in for ImageJ (National Institutes of Health, Bethesda, Md).

Western Blot Analysis

Western blot was performed as described previously[13] using primary antibodies against SMemb, calponin, mTOR, p-mTOR (Ser2448), eukaryotic translation initiation factor 4E-binding protein 1 (4E-BP1), and p-4E-BP1 (Ser65) (n = 5 in each group). A glyceraldehyde-3-phosphate dehydrogenase antibody was used as the gel loading control.

Statistical Analysis

All statistical tests were performed using JMP Pro version 12.2 (SAS Institute Inc, Cary, NC). Continuous variables are expressed as median (range) and compared using Wilcoxon rank-sum test. Multiple groups were compared by Kruskal-Wallis test, followed by post hoc analysis with Bonferoni correction.

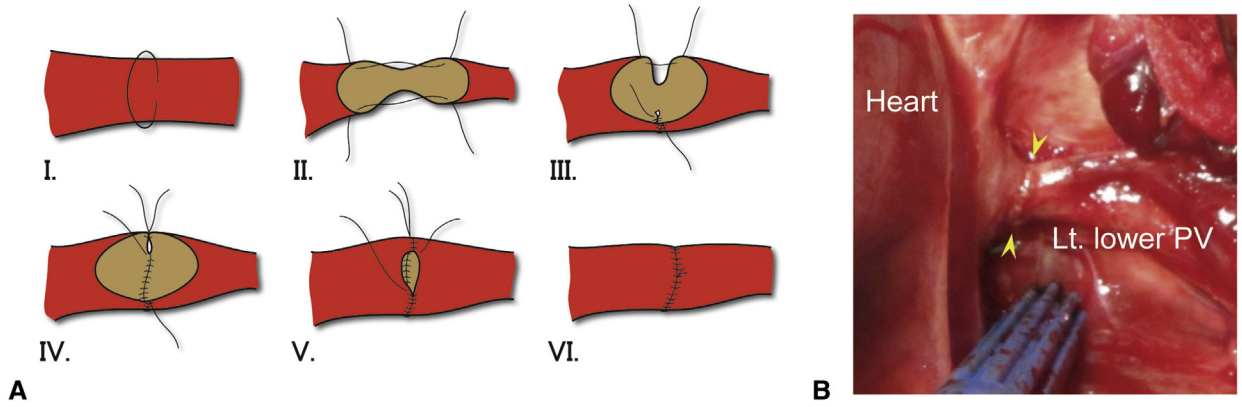

FIGURE 1. Surgical procedure. A, Diagram of the cut and suture technique applied to the left lower pulmonary vein (*PV*). The PV was transected subcircumferentially (I and II), and the entire circumference including the postpedicled portion were re-anastomosed with 7–0 Prolene running suture (III-VI). B, There was a slight purse string stricture at the anastomotic site of the left lower pulmonary vein (Lt. lower PV) (*yellow arrowhead*).

For analysis of PV patency rates, Kaplan-Meier curves were constructed for each group and compared by log-rank test. To correct for multiple testing, Bonferoni correction was applied as post hoc analysis.

RESULTS

Experiment I: Development of an Animal Model of PVO Progression

In the sham group, PV stenosis was not observed at least until 8 weeks postsurgery (Video 1, *A-D*), whereas anastomotic stenosis was detected as early as 1 week postsurgery in the PVO group. Stenosis gradually progressed in all 5 PVO model animals, and PVs could not be visualized angiographically by 3 weeks after the procedure (Video 2, *A-D*).

Temporal hemodynamic changes are shown in Table 1. Although no parameter differed significantly between sham and PVO groups at baseline, left pulmonary capillary wedge pressure (PCWP) was significantly elevated in the PVO group compared with the sham group at 1 week postsurgery (median, 10 mm Hg; range, 7-11 mm Hg vs median, 5 mm Hg; range, 4-8 mm Hg; $P = .048$). At 2 weeks postsurgery, left PCWP was even higher in the PVO group and slightly lower in the sham group (median, 10 mm Hg; range, 9-13 mm Hg vs median, 4; range, 4-5 mm Hg; $P = .01$). In addition, systolic pulmonary arterial blood pressure (PAP) and mean PAP were also significantly elevated in the PVO group compared with the sham group at 2 weeks postsurgery (median systolic PAP, 29 mm Hg; range, 22-40 mm Hg vs median, 18 mm Hg; range, 15-19 mm Hg; $P = .01$; median mean PAP, 22 mm Hg; range, 17-30 mm Hg vs median, 14 mm Hg; range, 13-15 mm Hg; $P = .01$). Moreover, systolic PAP, mean PAP, and left PCWP tended to continue to increase in the PVO group compared with the sham group at 8 weeks postsurgery (sham; n = 4, PVO; n = 3).

Vascular Remodeling at the Anastomotic Site

At 1 week postsurgery, fibrosis and neointimal lesions were not detected at the location corresponding to the PV intervention site in the sham group; however, those were apparent at the intervention site of the PVO groups (n = 5 in each group) (the upper row of Figure 3, *A*). Elastica-Masson staining confirmed fibromuscular intimal hyperplasia, and immunohistochemistry revealed that the neointimal lesion cells had greater expression of αSMA than in sham control PV. In addition, multiple Ki-67- and p-mTOR-positive cells were observed in the neointimal lesions at 1 week postsurgery, and these cells were doubly stained for αSMA plus Ki-67 (Figure 3, *B*) and αSMA plus p-mTOR (Figure 3, *C*).

At 8 weeks postsurgery, stenosis and intimal hyperplasia were not observed in the sham group (n = 4) at the PV segment corresponding to the anastomotic site in the PVO group (n = 5). In the PVO group, fibrotic lesions and anastomotic stenosis were observed (the lower row of Figure 3, *A*). Although PVs were not visualized by angiographic examinations at 8 weeks, macroscopic examination of resected PV revealed a pinhole lumen at the anastomotic site and advanced anastomotic stenosis in all animals. Furthermore, microscopic examinations revealed intimal fibrosis at the anastomotic site and infiltration of inflammatory cells around the suture (Figure 3, *A*).

Vascular Remodeling at the Upstream PVs

Intimal hyperplasia was evident at the upstream PVs in the PVO group (n = 5) even at 1 week postsurgery but not in the sham group (n = 5) (normalized intimal area [IA/R^2]: median, 0.10; range, 0.09-0.11 vs median, 0.07; range, 0.07-0.09; $P = .01$). This lesion was exacerbated by 8 weeks in the PVO group (n = 5) (1 week vs 8 weeks: median, 0.10; range, 0.09-0.11 vs median, 0.26; range, 0.24-0.40; $P = .01$) (Figure 4, *A*). More to the point, the intimal lesion was extensively developed towards the upstream PVs in the PVO group (Figure 4, *B*). On the other hand, intima-media thickness (MA/R^2) did not differ between the groups at 1 week. That significantly regressed in the sham group (median, 1.27; range, 0.86-1.30 vs

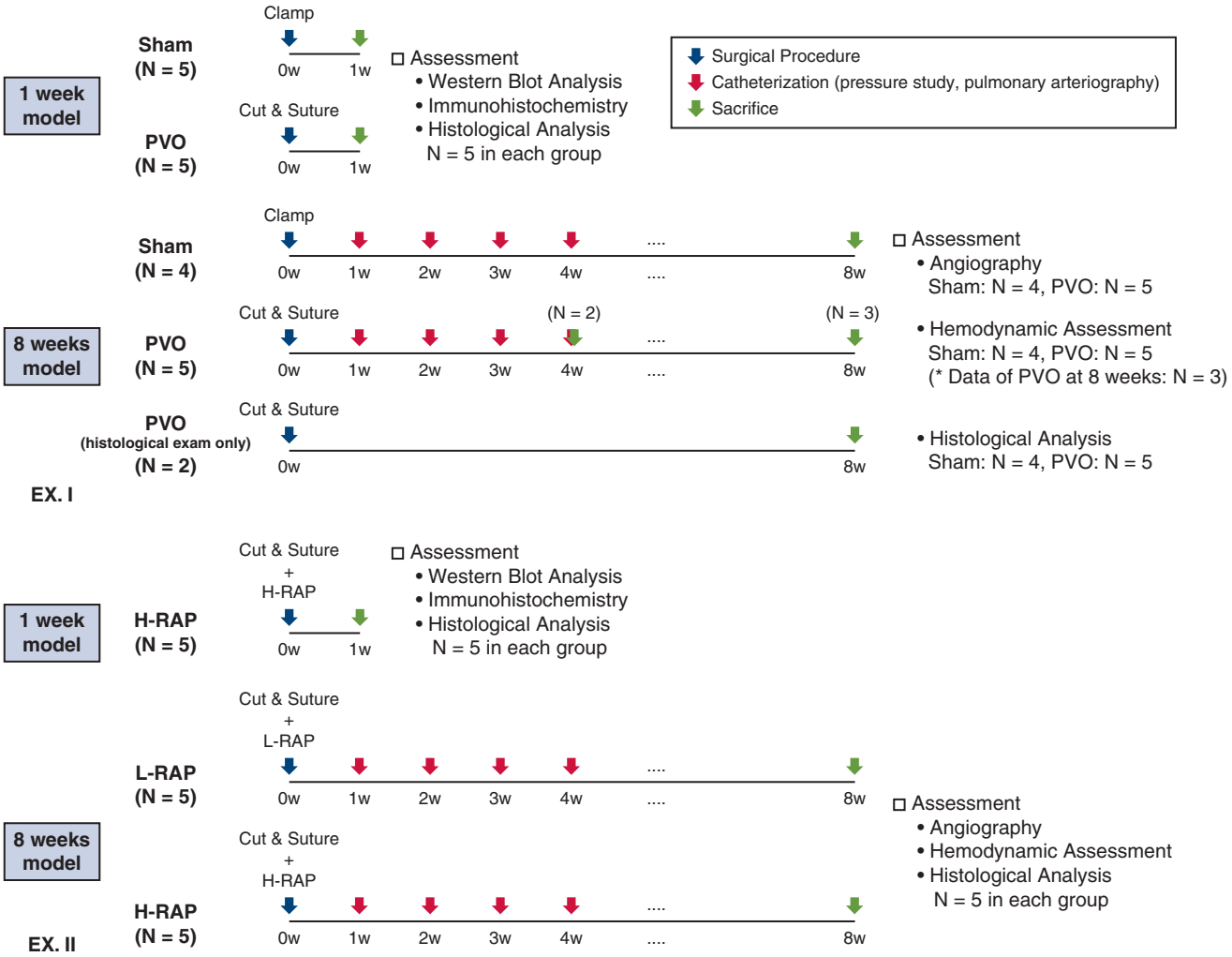

FIGURE 2. Study protocols. Experiment I (Ex. I) was designed to evaluate the similarity of the pulmonary vein obstruction (*PVO*) model to human PVO, and Experiment II (Ex. II) to evaluate the therapeutic potential of rapamycin film treatment. In the sham group (n = 4), the left lower PV was dissected from surrounding tissue and clamped for 20 to 25 minutes. In the PVO model groups (PVO modeling only, low-dose [*L-RAP*], and high-dose [*H-RAP*] rapamycin film treatment groups), the left lower PV was cut and re-anastomosed as in Figure 1, *A*. Pigs in the PVO-only group were killed at 1 week (n = 5), 4 weeks (n = 2), or 8 weeks (n = 5) postsurgery for histologic examination. Weekly catheter examinations of hemodynamic indices were performed until the anastomotic PV was no longer visible by angiography (except for 2 pigs used exclusively for histologic analysis at 8 weeks). Pigs in the L-RAP and H-RAP groups were likewise examined weekly for hemodynamic indices and then killed for histology at 1 week (H-RAP: n = 5), or 8 weeks (L-RAP: n = 5 and H-RAP: n = 5) after surgery and film implantation.

median, 0.67; range, 0.55-0.87; $P = .03$), whereas it progressed in the PVO group, and that was significantly higher in the PVO group than in the sham group at 8 weeks postsurgery (median, 1.94; range, 0.77-2.26 vs median, 0.67; range, 0.55-0.87; $P = .03$) (Figure 4, *A*).

Immunohistochemistry revealed that expression levels of αSMA, calponin, and h-caldesmon, markers of the contractile phenotype, were present in the intima-media of upstream PVs in both sham and PVO groups, but were diminished in the neointima of upstream PVs in the PVO group at 1 week. On the other hand, the expression of the synthetic phenotype marker of smooth muscle cells (SMCs), SMemb, was elevated in neointimal lesions of the PVO group compared to the intima-media. These findings in the PVO group are consistent even at 8 weeks. On the other hand, p-mTOR-positive cells and Ki-67-positive cells were detected in neointimal lesions of the PVO group at 1 week (the upper row of Figure 5, *A*); however, those were no longer present in the neointimal lesions of PVO group at 8 weeks (the lower row of Figure 5, *A*).

Western blot analysis (n = 5 in each group) revealed that upstream PVs in the PVO group had lower expression of calponin than the sham group (median, 3.1; range, 1.0-3.6 vs median, 4.7; range, 3.4-5.4; $P = .02$) and greater expression of SMemb (median, 3.3; range, 1.7-4.0 vs median, 1.6; range, 0.9-1.9; $P = .02$) than sham controls. Additionally,

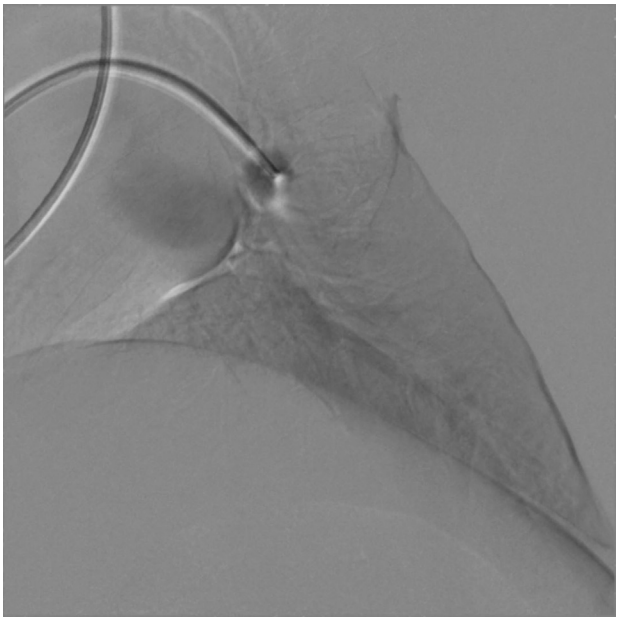

VIDEO 1A. Postoperative pulmonary angiographic video in sham group. The image was acquired immediately after the operation. Video available at: https://www.jtcvs.org/article/S0022-5223(20)30505-5/fulltext.

levels of phosphorylated mTOR and 4E-BP1 were higher in the upstream PV of the PVO group than in the sham group (mTOR: median, 0.21; range, 0.16-0.24 vs median, 0.15; range, 0.11-0.20; $P = .04$) and 4E-BP1: (median, 0.36; range, 0.32-0.46 vs median, 0.28; range, 0.21-0.32; $P = .02$) (Figure 5, *B*).

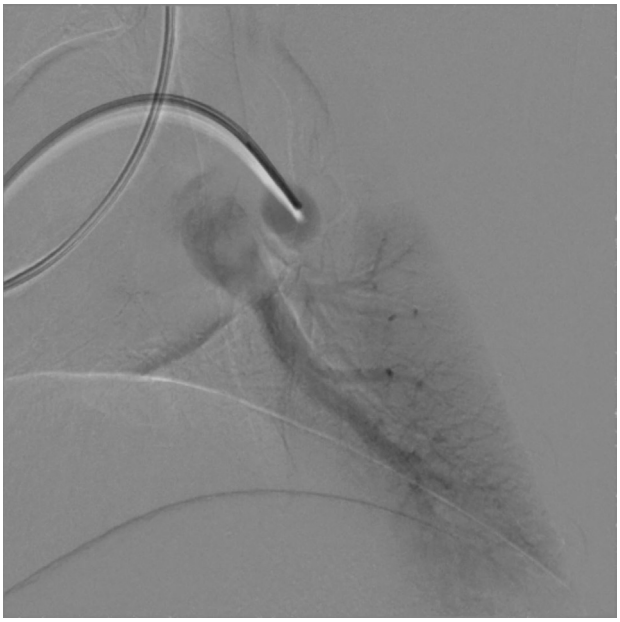

VIDEO 1B. Postoperative pulmonary angiographic video in sham group. The image was acquired immediately 1 week after the operation. Video available at: https://www.jtcvs.org/article/S0022-5223(20)30505-5/fulltext.

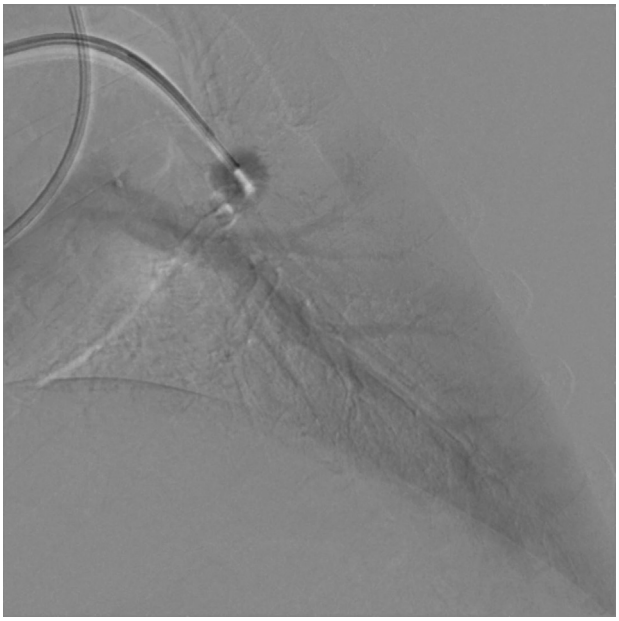

VIDEO 1C. Postoperative pulmonary angiographic video in sham group. The image was acquired 2 weeks after the operation. Video available at: https://www.jtcvs.org/article/S0022-5223(20)30505-5/fulltext.

Experiment II: Rapamycin-Eluting Films Prevent Stenosis at the PV Anastomotic Site

At 1 week after the procedure, anastomotic stenosis was mitigated in the H-RAP group compared with the PVO group (n = 5 in each group) (IA/R^2: median, 0.12; range, 0.05-0.16 vs median, 0.18; range, 0.13-0.60;

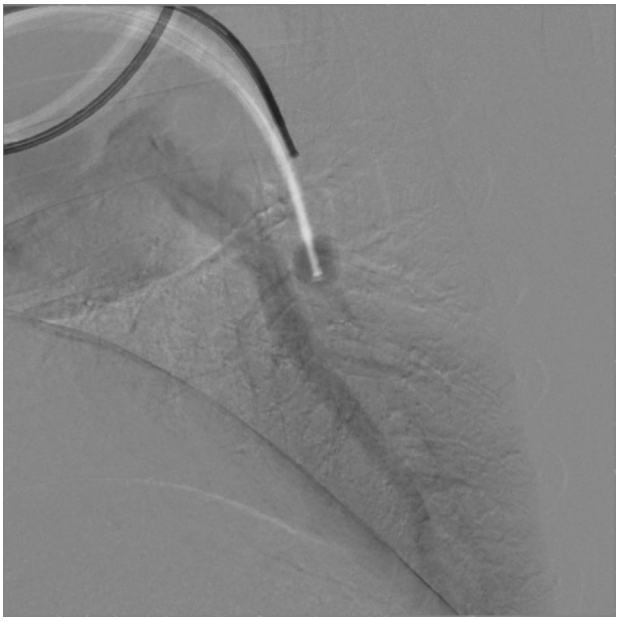

VIDEO 1D. Postoperative pulmonary angiographic video in sham group. The image was acquired immediately 3 weeks after the operation. Washout of radiopaque dye was observed even at 3 weeks postsurgery, indicating no stenosis at the intervention site. Video available at: https://www.jtcvs.org/article/S0022-5223(20)30505-5/fulltext.

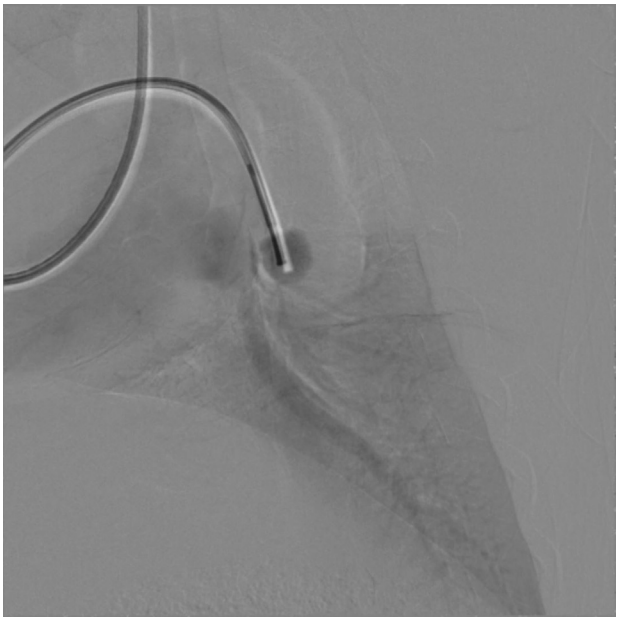

VIDEO 2A. Postoperative pulmonary angiographic video in PVO group. Immediately after the operation, the PV was patent. Video available at: https://www.jtcvs.org/article/S0022-5223(20)30505-5/fulltext.

$P = .048$), and progression of intimal hyperplasia at a 6-mm distance from the anastomotic site was significantly less severe in the H-RAP group (median, 0.04; range, 0.02-0.05 vs median, 0.06; range, 0.05-0.14; $P = .03$) (Figure 6, *A*). In addition, the Ki-67-positive cell ratio in the neointima tended to be lower (median, 0.09; range,

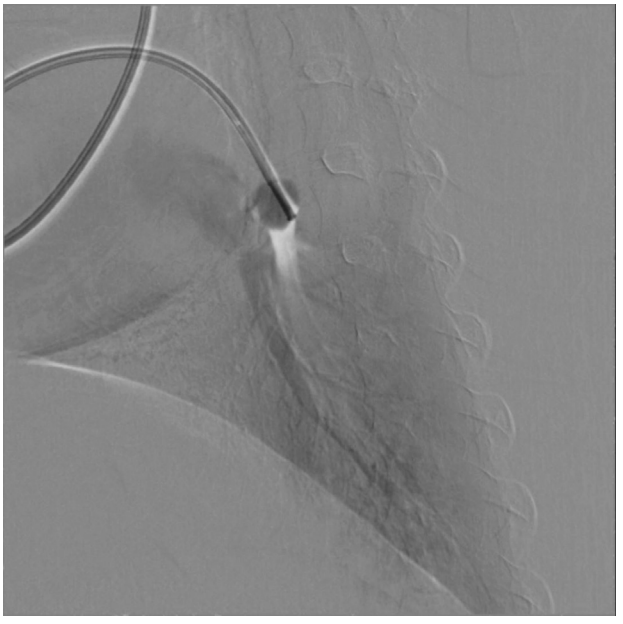

VIDEO 2B. Postoperative pulmonary angiographic video in PVO group. After 1 week, the PV was still patent but slightly narrow, and accelerated flow was observed. Video available at: https://www.jtcvs.org/article/S0022-5223(20)30505-5/fulltext.

VIDEO 2C. Postoperative pulmonary angiographic video in PVO group. At 2 weeks, stenosis at the anastomotic site had progressed. Washout of pulmonary arterial flow and drainage from the pulmonary vein became slower. Video available at: https://www.jtcvs.org/article/S0022-5223(20)30505-5/fulltext.

0.02-0.14 vs median, 0.16; range, 0.08-0.23; $P = .11$), and p-mTOR-positive cell ratio significantly diminished in the H-RAP group compared with the PVO group

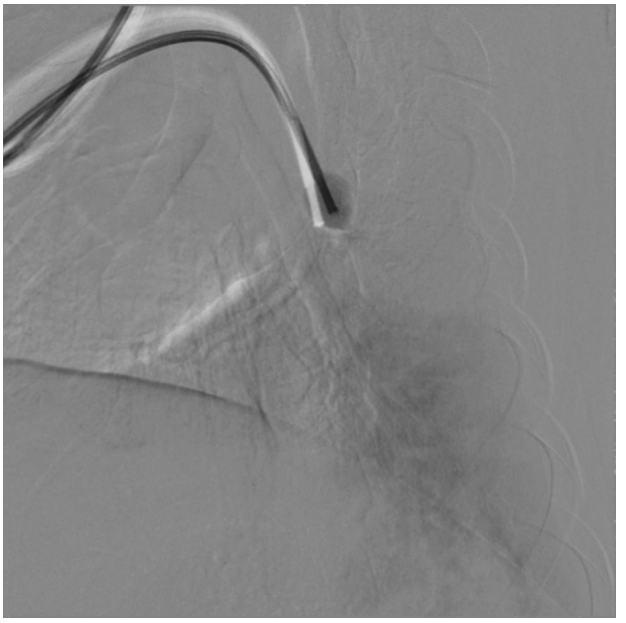

VIDEO 2D. Postoperative pulmonary angiographic video in PVO group. At 3 weeks, washout of pulmonary arterial flow worsened compared to that at 2 weeks, and pulmonary venous drainage was no longer visible as dye washout. Video available at: https://www.jtcvs.org/article/S0022-5223(20)30505-5/fulltext.

TABLE 1. Hemodynamic data obtained at each time point

Time (wk)	Weight (kg)	HR (bpm)	sABP (mm Hg)	mABP (mm Hg)	sPAP (mm Hg)	mPAP (mm Hg)	sPp/Ps	mPp/Ps	CVP (mm Hg)	RPCWP (mm Hg)	LPCWP (mm Hg)	CI (L/min/m^2)
Sham (n = 4)												
0	17 (16-18)	122 (115-127)	94 (89-104)	70 (62-79)	21 (20-22)	16 (15-17)	0.22 (0.21-0.25)	0.23 (0.20-0.27)	4 (4-5)	6 (5-6)	5 (5-6)	7.6 (5.8-7.6)
1	20 (15-20)	116 (96-120)	91 (88-98)	67 (59-75)	20 (17-25)	17 (15-19)	0.21 (0.19-0.27)	0.26 (0.23-0.27)	5 (3-5)	5 (4-7)	5 (4-8)	6.5 (5.3-7.3)
2	23 (23-24)	121 (113-127)	93 (88-100)	73 (65-76)	18 (15-19)	14 (13-15)	0.18 (0.16-0.21)	0.19 (0.17-0.23)	4 (3-4)	4 (3-5)	4 (4-5)	8.5 (7.4-9.2)
8	60 (58-62)	109 (104-115)	111 (109-120)	80 (78-83)	22 (16-23)	15 (13-18)	0.19 (0.13-0.21)	0.18 (0.16-0.23)	4 (4-6)	6 (5-7)	6 (4-7)	7.2 (6.3-9.9)
Pulmonary valve obstruction (n = 5)												
0	20 (15-22)	118 (105-130)	95 (84-102)	68 (63-85)	20 (19-27)	16 (15-19)	0.23 (0.20-0.28)	0.23 (0.20-0.28)	4 (3-5)	5 (4-6)	5 (4-5)	7.0 (5.9-8.1)
1	22 (19-26)	115 (100-130)	92 (90-110)	70 (64-91)	26 (23-28)	19 (15-21)	0.25 (0.23-0.31)	0.23 (0.19-0.33)	4 (2-5)	6 (4-9)	10 (7-11)*	6.0 (5.3-6.2)
2	25 (23-30)	120 (98-130)	105 (93-110)	78 (58-90)	29 (22-40)*	22 (17-30)*	0.29 (0.20-0.42)	0.29 (0.19-0.51)	5 (5-10)*	6 (5-11)*	10 (9-13)*	6.3 (6.3-7.8)
8†	57 (44-68)	93 (87-100)	101 (99-111)	75 (72-86)	29 (26-31)	22 (20-24)	0.29 (0.23-0.31)	0.28 (0.26-0.32)	6 (5-7)	7 (6-7)	10 (9-14)	5.3 (3.7-9.4)
L-RAP (n = 5)												
0	20 (13-22)	107 (104-130)	93 (87-111)	70 (58-95)	22 (19-28)	18 (15-20)	0.22 (0.21-0.27)	0.24 (0.20-0.26)	5 (4-6)	6 (3-6)	5 (4-6)	7.1 (5.5-8.9)
1	24 (16-25)	115 (106-124)	105 (91-108)	81 (68-85)	27 (23-33)	22 (18-23)	0.25 (0.24-0.35)	0.26 (0.25-0.29)	5 (3-8)	6 (4-7)	7 (5-9)	6.0 (5.9-7.7)
2	28 (20-30)	108 (96-135)	102 (100-108)	80 (74-83)	26 (24-34)	19 (16-24)	0.26 (0.22-0.32)	0.26 (0.20-0.29)	5 (4-7)	6 (4-8)	9 (5-11)	6.3 (5.1-6.9)
8	60 (44-72)	97 (89-110)	112 (92-128)	87 (69-107)	33 (26-38)	24 (20-28)	0.28 (0.26-0.41)	0.25 (0.24-0.40)	7 (5-7)	6 (6-8)	10 (8-13)	5.8 (5.4-6.6)
H-RAP (n = 5)												
0	18 (13-19)	113 (110-150)	101 (93-106)	77 (69-88)	22 (20-24)	16 (14-20)	0.22 (0.20-0.24)	0.20 (0.18-0.25)	4 (3-5)	5 (5-6)	5 (5-6)	7.9 (6.0-9.2)
1	21 (15-22)	110 (98-117)	96 (84-129)	70 (64-89)	25 (20-29)	17 (14-21)	0.23 (0.19-0.35)	0.21 (0.19-0.33)	5 (3-6)	7 (3-7)	6 (3-8)	6.5 (5.4-7.6)
2	24 (18-28)	108 (103-116)	94 (90-113)	75 (68-76)	22 (20-28)	17 (15-18)	0.23 (0.19-0.30)	0.22 (0.20-0.24)	5 (3-7)	5 (4-7)	8 (4-8)‡	6.6 (5.8-8.3)
8	57 (56-59)	98 (92-108)	111 (108-113)	81 (75-88)	27 (24-32)	20 (18-21)	0.24 (0.21-0.29)	0.23 (0.22-0.28)	5 (5-6)	7 (7-8)	12 (10-14)	5.8 (5.6-7.7)

Values are presented as median (range). *HR*, Heart rate; *sABP*, systolic arterial blood pressure; *mABP*, mean arterial blood pressure; s*PAP*, systolic pulmonary artery pressure; m*PAP*, mean pulmonary artery pressure; *Pp/Ps*, pulmonary artery pressure to systemic arterial blood pressure ratio; *CVP*, central venous pressure; *RPCWP*, right pulmonary capillary wedge pressure; *LPCWP*, left pulmonary capillary wedge pressure; *CI*, cardiac index. *$P < .05$ versus sham. †n = 3. ‡$P < .01$ versus PVO.

(median, 0.61; range, 0.51-0.69 vs median, 0.78; range, 0.62-0.83; $P = .03$) (Figure 6, *B*).

We also evaluated the suppressive effect of rapamycin-eluting films on anastomotic stenosis in the L-RAP and H-RAP groups (n = 5 in each group). The time course to PV occlusion in the L-RAP group did not differ from the PVO group ($P = .24$), but that in the H-RAP group was significantly longer than the PVO group ($P = .008$). However, even in the H-RAP group, PVs were eventually occluded by 8 weeks postsurgery in all animals (Figure 6, *C*).

Hemodynamic assessments indicated that L-RAP had no impact on hemodynamic changes compared with the PVO. Although there were also no differences in blood pressure values between H-RAP and PVO groups at 8 weeks postsurgery, left PCWP was significantly lower at 2 weeks in the H-RAP group than in the PVO group (median, 8; range, 4-8 vs median, 10; range, 9-13; $P = .01$). Additionally, mean PAP tended to be lower at 2 weeks in the H-RAP group than in the PVO group (median, 17; range, 15-18 vs median, 22; range, 17-30; $P = .03$; significance accepted at $P = .016$) (Table 1).

DISCUSSION

A Novel Pig PVO Model Mimicking Human PVO

In human PVO, pulmonary arterial hypertension and elevation of PCWP are the major hemodynamic changes,

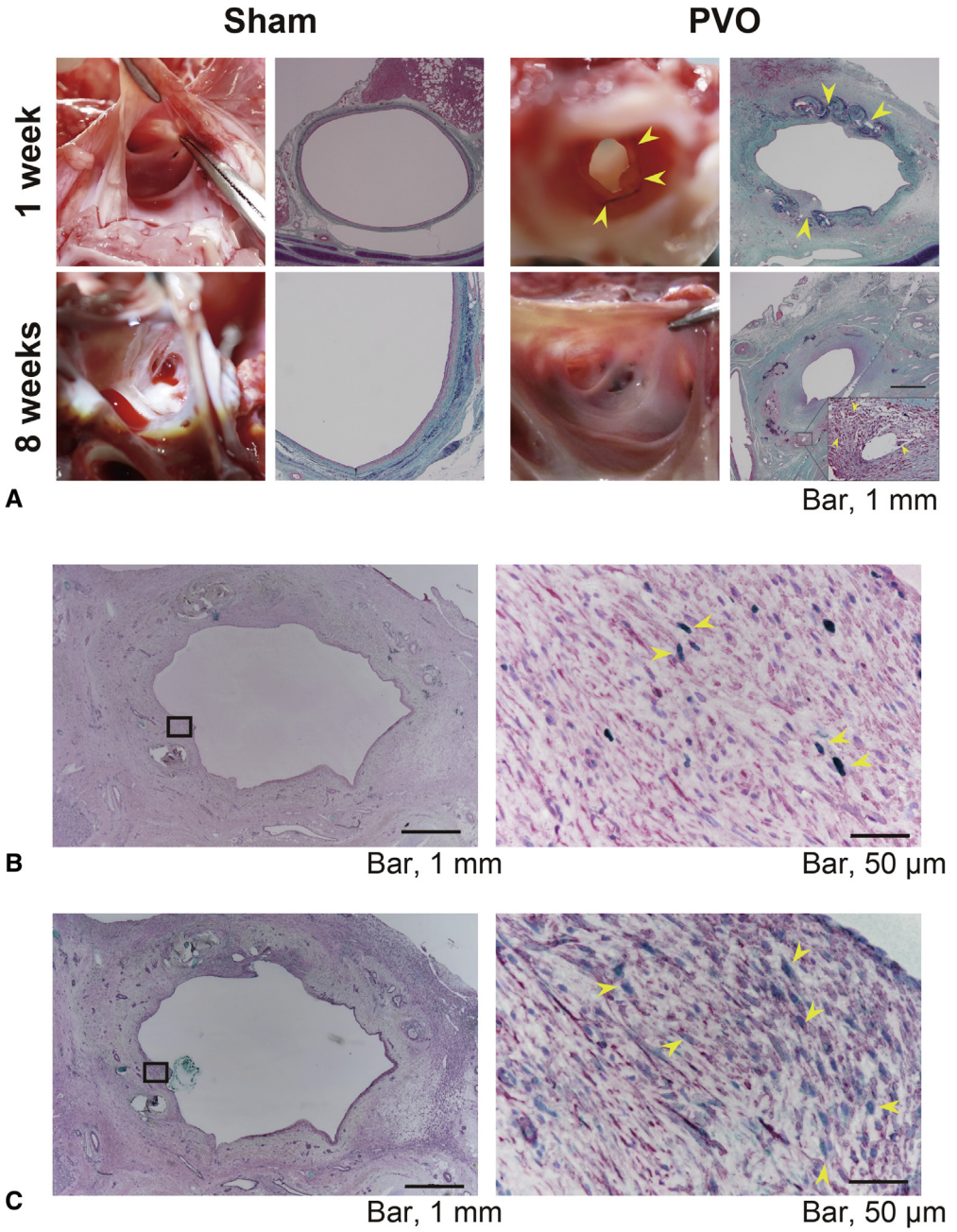

FIGURE 3. Vascular remodeling at the anastomotic site. A, Comparison of pulmonary vein (PV) histology between the anastomotic site of the pulmonary vein obstruction (*PVO*) model group and the corresponding site of the sham group. Intimal hyperplasia and luminal stenosis were not observed in the sham group even at 8 weeks. On the other hand, fibromuscular intimal hyperplasia and luminal stenosis were observed in the PVO group at 1 week, and intimal fibrosis and luminal stenosis were exacerbated at 8 weeks. Also, inflammatory cells infiltrated around the suture material (*arrowheads*). 20× magnification. B, Double immunostaining for α-smooth muscle actin (αSMA) and Ki-67 in the neointimal lesion at 1 week postsurgery of the PVO group demonstrated that Ki-67-positive proliferating cells were mainly αSMA-positive smooth muscle-like cells (*arrowheads*). C, Double staining for αSMA and phospho-mammalian target of rapamycin (p-mTOR) in neointimal lesions of PVO group PVs demonstrated that p-mTOR-positive cells were also mainly αSMA-positive smooth muscle-like cells (*arrowheads*). B and C, *left panels*: 20× magnification, and *right panels*: the enlarged areas of a box in the left panels at 400× magnification.

whereas intimal hyperplasia at the anastomotic site and progression to upstream PVs are cardinal histopathologic findings.[1,3,4,14] In addition, previous human studies reported that the main lesion cells in the neointima were αSMA-positive and did not express endothelial markers (CD31 or von Willebrand factor).[9,15] These hemodynamic and histopathologic changes were also detected in this pig PVO model. Thus, our pig PVO model replicates the major

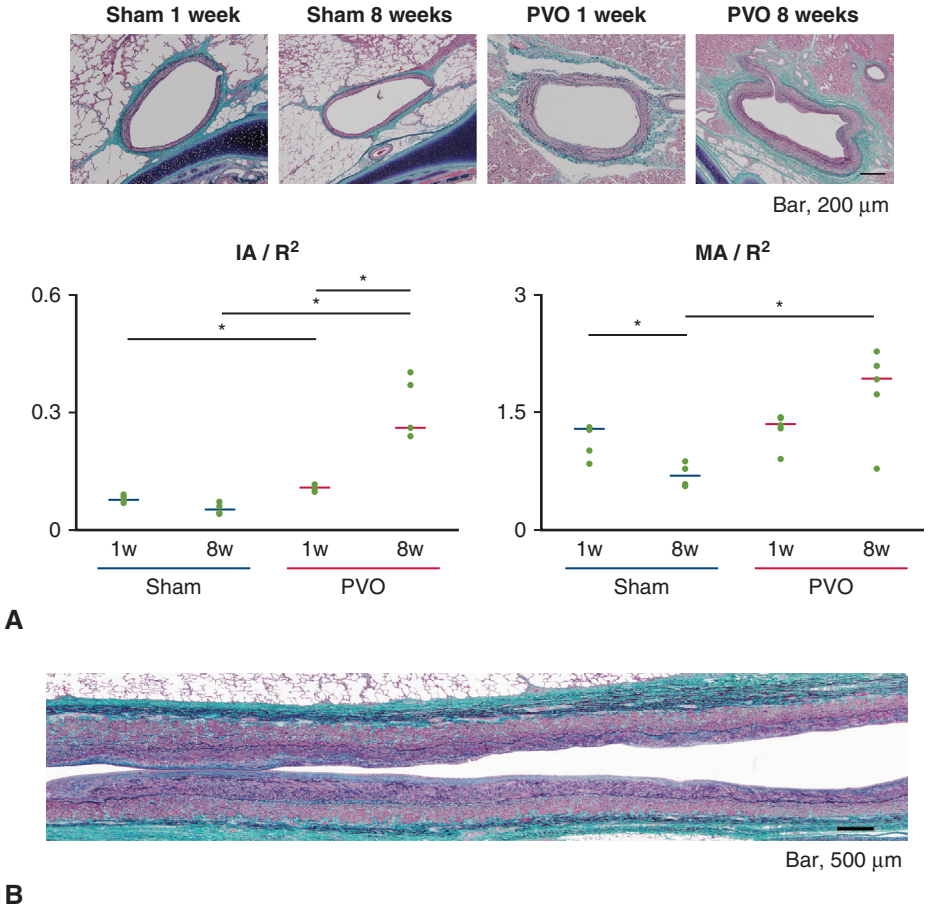

FIGURE 4. Vascular remodeling at the upstream pulmonary veins (PVs). A, Histological features of the upstream PV in sham and pulmonary vein obstruction (*PVO*) groups (100× magnification). Bars indicated median in each group, and plots indicated each measurement. Normalized intimal area (IA/R^2) was significantly higher in the PVO group compared with the sham group even at 1 week. IA/R^2 was unchanged in the sham group at 8 weeks; however, that was significantly progressed at 8 weeks in the PVO group. Normalized intima-media area (MA/R^2) in the PVO group was similar to the sham group at 1 week; however, that significantly regressed in the sham group, although it tended to be thickened in the PVO group. MA/R^2 in the PVO group at 8 weeks was significantly higher than that in the sham group (*$P < .05$). B, Long axis view of the upstream PV in the PVO group in low magnification (40× magnification).

cellular and functional abnormalities of post-TAPVC human PVO.

Pathophysiology of the Anastomotic Stenosis

Studies of PVO after TAPVC repair have reported intimal hyperplasia and luminal stenosis at the anastomotic site.[1,3,14] However, histopathologic changes at the anastomotic site have not been described. Proposed causes of intimal hyperplasia and anastomotic stenosis include organic stenosis and turbulent flow effects due to incomplete anastomotic techniques,[8,16] direct tissue injury from the operative techniques (eg, clamping and holding PVs during anastomosis),[8,17] nongrowth and constriction of the anastomotic site due to nonabsorbable sutures,[18] and pre-existing pathologic changes in the left atrial and pulmonary venous tissues of TAPVC patients.[19] In our pig PVO model, the diameter of anastomotic PVs immediately postsurgery was approximately 70% of that before the procedure, indicating that organic stenosis had a greater influence on anastomotic intimal hyperplasia than direct tissue injury from clamping or vessel manipulation during the operation. In addition, infiltration of inflammatory cells around the suture material was observed at both 1 and 8 weeks, suggesting that inflammation caused by the suture string also contributed to anastomotic remodeling. Moreover, phosphorylation (Ser2448) of mTOR and nuclear translocation in SMC-like cells of the neointima at the anastomotic site were observed in the PVO group. Activation of the mTOR pathway is a key pathogenic event in coronary artery stent restenosis,[20] atherosclerotic changes,[21] and pulmonary arteriopathic lesions associated with pulmonary arterial hypertension.[22] Li and colleagues[23] reported that the mTOR pathway regulates the remodeling of vein grafts in a mouse model of coronary artery bypass. The results of the present study suggest that activation of the mTOR

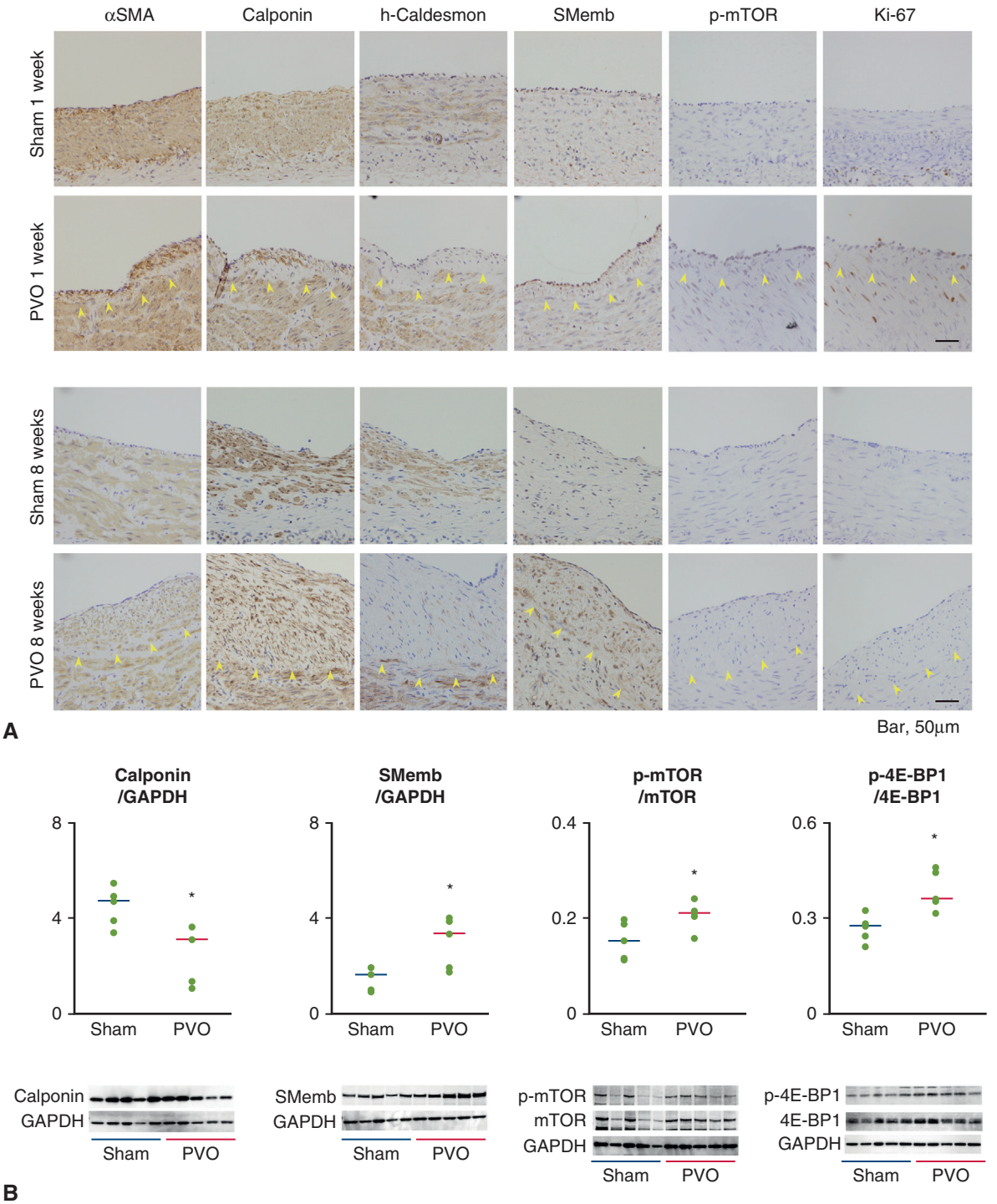

FIGURE 5. Histochemical features and protein expression patterns of the upstream pulmonary veins (PVs). A, Comparison of immunohistochemical expression patterns in upstream PVs between groups at 1 week and 8 weeks postsurgery. The arrowheads indicated the internal elastic lamina (400× magnification). At 1 week, lesional cells in the neointima of the pulmonary vein obstruction (*PVO*) group exhibited weak α-smooth muscle actin (*αSMA*) expression. These smooth muscle-like cells also exhibited reduced expression of differentiated smooth muscle cell (SMC) markers (calponin and h-caldesmon) and greater expression of the dedifferentiated SMC marker nonmuscle myosin heavy chain (*SMemb*) compared with the sham control. These findings were consistent at 8 weeks. Cells positive for phosphorylated mammalian target of rapamycin (*p-mTOR*) were abundant in the neointima, and those positive for Ki-67 were also observed at 1 week, yet, no longer observed at 8 weeks. B, Western blot analysis. *Bars* indicate median in each group, and *plots* indicate each measurement. Upstream PV tissue from the PVO group showed lower expression of calponin and greater expression of SMemb compared with the sham group. p-mTOR and phosphorylated eukaryotic translation initiation factor 4E-binding protein 1 (*p-4E-BP1*) were elevated in the PVO group compared to the sham group (*$P < .05$). *GAPDH*, Glyceraldehyde 3-phosphate dehydrogenase.

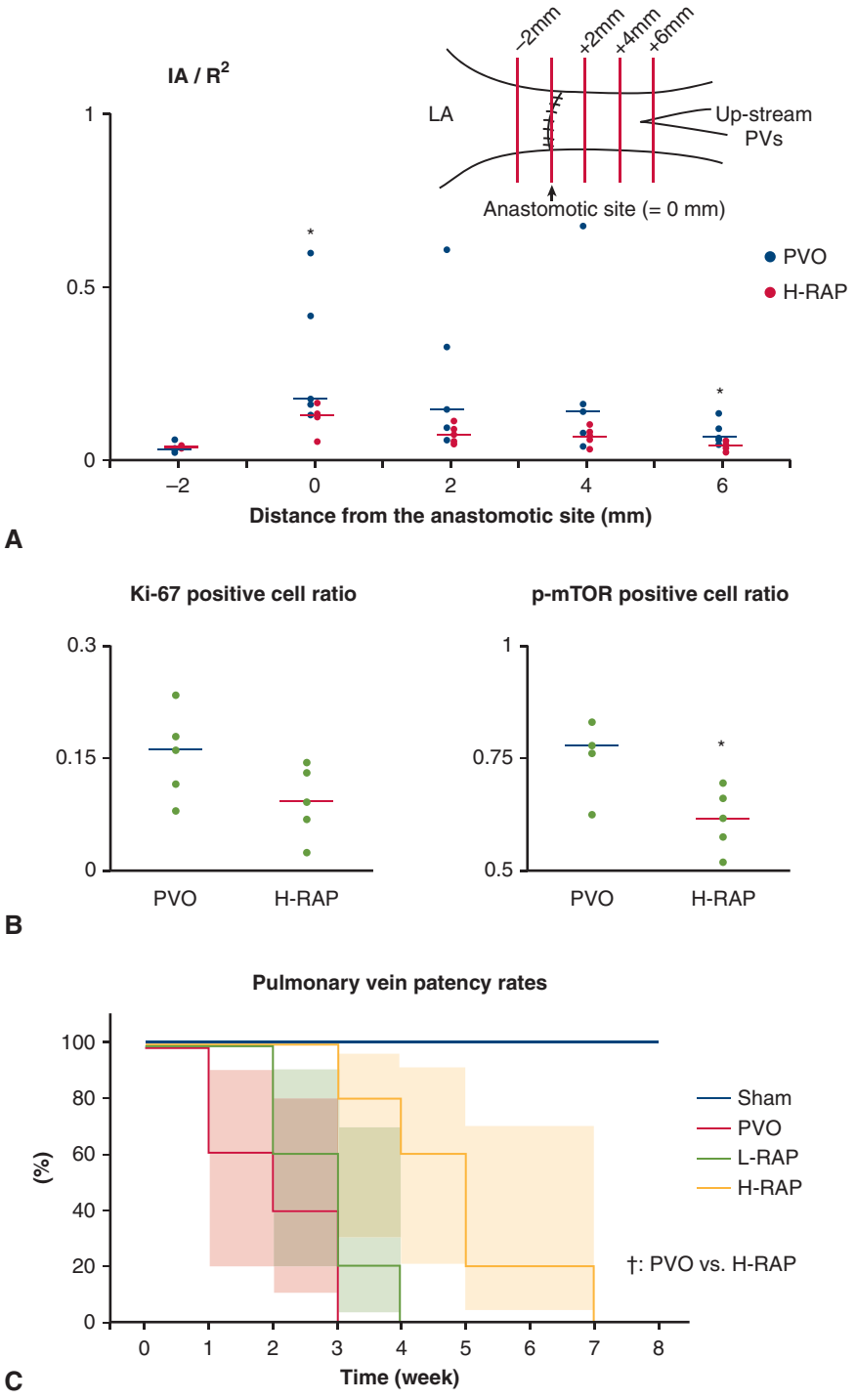

FIGURE 6. Evaluation of rapamycin-eluting film treatment. A, high-dose rapamycin film (*H-RAP*) markedly reduced normalized intimal area (IA/R^2) from the anastomotic site to the upstream site (*$P < .05$). B, *Bars* indicate median in each group, and *plots* indicate each measurement. The Ki-67-positive cell ratio tended to be lower in the H-RAP group ($P = .06$). In addition, the ratio of phosphorylated mammalian target of rapamycin (*p-mTOR*)-positive cells to mTOR-positive cells was significantly lower in the H-RAP group (*$P < .05$). C, Kaplan-Meier curves of anastomotic pulmonary vein (PV) patency rates. There was no significant difference between the low-dose rapamycin film treatment group (*L-RAP*) and the pulmonary vein obstruction (*PVO*) group. However, H-RAP treatment extended the time course until anastomotic PV occlusion compared with the PVO group. (†$P < .01$).

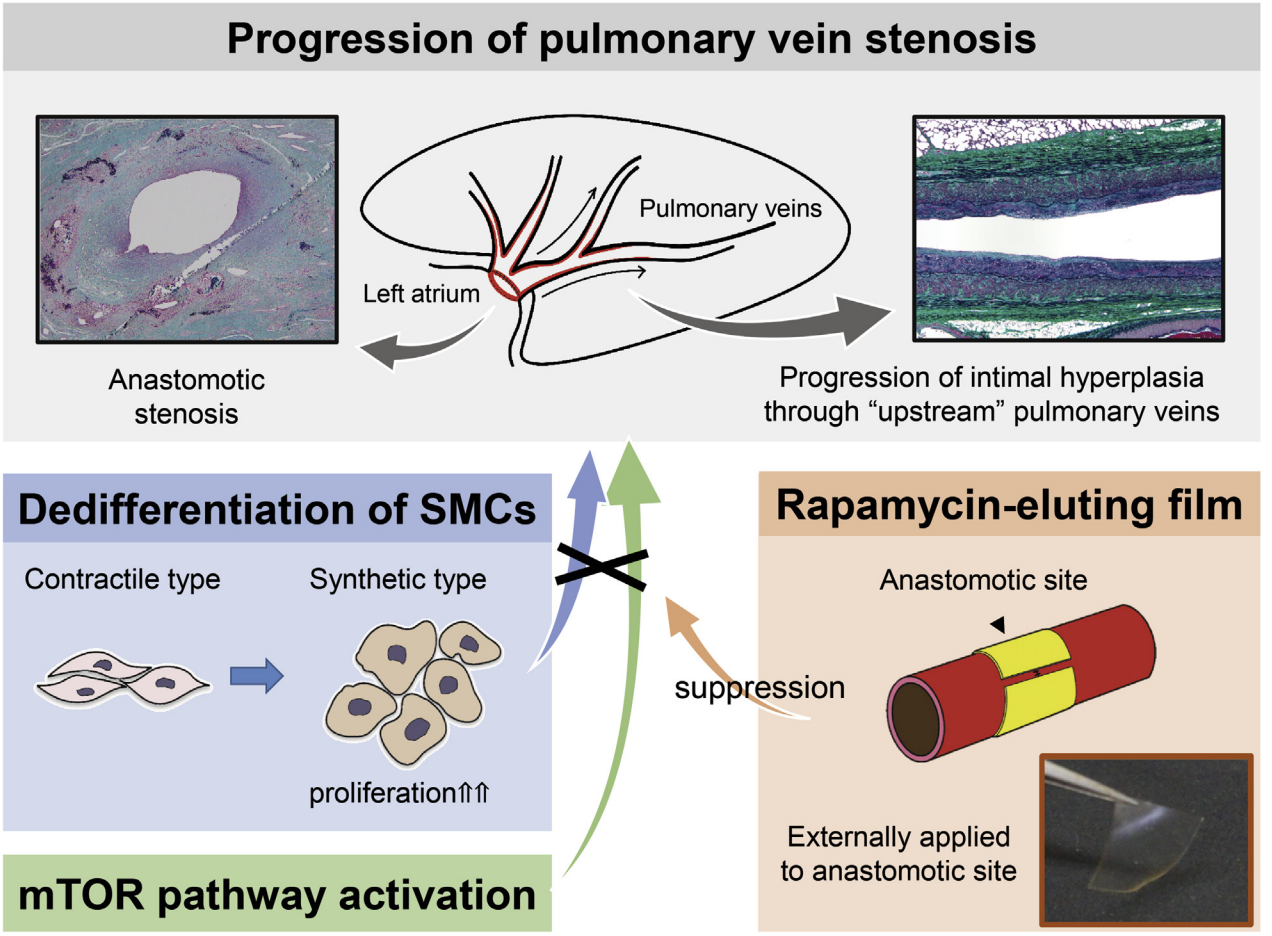

FIGURE 7. Dedifferentiation of smooth muscle cell (*SMC*)-like cells and mammalian target of rapamycin (*mTOR*) pathway activation appeared to be involved in the pathogenesis of pulmonary vein obstruction (PVO) progression. Local delivery of rapamycin to the anastomotic site from the external side delayed pulmonary vein (PV) anastomotic stenosis implicating a new therapeutic strategy to prevent PVO progression.

pathway is also critical for intimal hyperplasia and SMC-like cell proliferation associated with pulmonary venous anastomotic remodeling.

Progression of Vascular Remodeling Toward Upstream PVs

In the present study, intimal hyperplasia always progressed to upstream PVs, in accord with both histologic changes in human PVO[1] and a pig banding PVO model.[9,10] Even at 1 week postsurgery, intimal hyperplasia was evident toward upstream PVs in PVO group, and these intimal lesions were further exacerbated at 8 weeks postsurgery with resultant anastomotic occlusion. These facts indicated that the mechanical stricture of anastomotic site would be one of the most important key factors for vascular remodeling of upstream PVs as well as anastomotic site. We also observed increased phosphorylation of mTOR and 4E-BP1 in upstream PVs. These findings strongly suggest that the mTOR signaling pathway contributes to remodeling of upstream PVs. Many studies have reported that the mTOR pathway regulates the proliferation of SMCs during vascular remodeling,[20-23] but this is the first report implicating mTOR pathway activation in the progression of PVO. Kato and colleagues[9] reported that upstream PV in the pig banding PVO model exhibited greater expression of transforming growth factor-beta1 (TGF-β1) and Smad4, and that ensuing endothelium to mesenchymal transition was a key factor in the progression of intimal hyperplasia to upstream PVs. However, in a recent report from the same research group, significant elevation of TGF-β1 was not observed,[11] thus, the contribution of the TGF-β/Smad pathway to PVO progression is still undetermined.

Riedlinger and colleagues[24] reported that the predominant lesion cells in the neointima of congenital PVO were myofibroblasts with characteristics of both fibroblasts and SMCs. They also reported paracrine or autocrine roles for growth factors, such as platelet-derived growth factor and fibroblast growth factor, in the pathogenesis of intimal occlusive lesions. In the present study, lesion cells had characteristics of the synthetic phenotype SMCs, which

resemble myofibroblasts.[25] Because the mTOR pathway is positioned downstream from growth factors signaling, it is conceivable that growth factors are involved in the progression of PV remodeling through mTOR activation.

Prevention of Anastomotic Stenosis by Rapamycin-Eluting Films

Our preliminary study revealed a transient suppressive effect of rapamycin-eluting films on anastomotic stenosis in PVO. Rapamycin is known to suppress cell proliferation, and its derivatives and functional analogs (mTOR inhibitors) have been tested extensively as antitumor drugs.[26] Furthermore, rapamycin shifts the cytokine release profile from pro- to anti-inflammatory, and so has been used as an immunosuppressant in drug-eluting stents for angioplasty.[27,28] Rapamycin binds to a domain separate from the catalytic site to block a subset of mTOR functions.[29] Among the effects of mTOR blockade, phosphorylation of 4E-BP1 and ribosomal protein S6 kinase 1 are reduced, which results in inhibition of global protein translation and cell cycle arrest.[30] Hu and colleagues[31] demonstrated that platelet-derived growth factor induced the phenotypic transition of SMCs from contractile type to synthetic type, and that this change could be suppressed by rapamycin. In addition, rapamycin has been reported to suppress SMC migration.[32] These effects could contribute to the suppressive effect of rapamycin on intimal hyperplasia and its progression. We previously demonstrated that external application of rapamycin-eluting film prevents intimal hyperplasia in a vascular anastomosis model.[12] In the present study, we applied rapamycin-eluting film to the PV anastomotic site externally and observed reduced SMC-like cells proliferation (as evidenced by reduced Ki-67 expression), presumably due to mTOR inhibition.

We tested 2 different doses of rapamycin, 1 mg (L-RAP) and 10 mg (H-RAP). The lower dose is approximately equivalent to that in rapamycin-eluting stents (140 μg rapamycin in 1 cm^2 of stent area).[12,28] Although L-RAP did not achieve any significant suppressive effect on anastomotic stenosis, a 10-fold higher concentration could suppress intimal hyperplasia at the anastomotic site and prolonged the time course to PV occlusion. This ameliorative effect was transient; however, as PV stenosis and occlusion were eventually observed after 8 weeks. In our previous report, rapamycin film treatment was less effective on arterial–venous anastomosis than arterial–arterial anastomosis.[12] Clinically, the patency of vein grafts following coronary artery bypass is lower than arterial grafts, suggesting that the reaction of SMCs may differ during vascular remodeling between arteries and veins. In addition, Wang and colleagues[33] reported that rapamycin treatment was less effective on vein grafts than arterial grafts, and suggested that the difference in therapeutic efficacy was due to the timing of mTOR pathway activation. If mTOR activation is delayed in veins, the dose delivered at peak activation may be insufficient for full pathway suppression. Thus, differences in SMC reactivity between arteries and veins could be 1 reason that high-dose rapamycin treatment was only transiently effective for preventing PV anastomotic stenosis. An even higher dose or more sustained release may be needed to achieve complete prevention of PV anastomotic stenosis.

Study Limitations

In the present study, we established a novel pig PVO model by cutting and sewing the left lower PV. In this model, we created the isolated PVO localized in the single left lower PV, not in all PVs. This is different from the human clinical setting and among the limitations of this study. In terms of compatibility of our present model with human PVO, we could obtain a peripheral lung specimen from a human PVO patient and confirm the similarity of the histopathologic and immunohistochemical changes at the upstream PVs between human and pig PVO model (data not shown). However, we could not obtain enough lung specimens of the human PVO patient. Further study is warranted for comparison of the histopathologic and immunohistochemical changes between human and this pig PVO model. In addition, our study of rapamycin-eluting films did not include a group treated with rapamycin-free polylactide-co-glycolide films as a control, although we included a low-dose group. And we did not include the L-RAP group in the comparative study protocol for 1 week model in view of reduction of the number of animals that were put to death. Moreover, we did not prepare frozen sections for immunofluorescence assessment, and we could not perform double staining with p-mTOR and Ki-67 using immunofluorescence. Therefore we could not show evidence that is more convincing to prove direct association between mTOR activation and SMC proliferation.

CONCLUSIONS

We established a novel pig PVO model using a cut and suture technique that mimicked many hemodynamic and histopathologic features of human PVO. The predominant lesion cells in the neointima were SMC-like cells of the synthetic phenotype, and activation of the mTOR pathway appeared to contribute to the proliferation of these cells and the progression of vasculopathy toward upstream PVs. In addition, activation of mTOR was also observed in SMC-like cells at the anastomotic site. Rapamycin-eluting films applied externally to the anastomotic site transiently suppressed stenosis in this model. Thus, this therapeutic material could present a new therapeutic option for the prevention of PVO following TAPVC repair (Figure 7).

Conflict of Interest Statement

Authors have nothing to disclose with regard to commercial support.

The authors thank Ayako Ono for assistance in animal experiments, Teruko Sueta for management of animals, and Fumiko Date for performing the histologic staining.

References

1. van de Wal HJ, Hamilton DI, Godman MJ, Harinck E, Lacquet LK, van Oort A. Pulmonary venous obstruction following correction for total anomalous pulmonary venous drainage: a challenge. *Eur J Cardiothorac Surg*. 1992;6:545-9.
2. Seale AN, Uemura H, Webber SA, Partridge J, Roughton M, Ho SY, et al. Total anomalous pulmonary venous connection: outcome of postoperative pulmonary venous obstruction. *J Thorac Cardiovasc Surg*. 2013;145:1255-62.
3. Lacour-Gayet F, Zoghbi J, Serraf AE, Belli E, Piot D, Rey C, et al. Surgical management of progressive pulmonary venous obstruction after repair of total anomalous pulmonary venous connection. *J Thorac Cardiovasc Surg*. 1999;117:679-87.
4. Ricci M. Management of pulmonary venous obstruction after correction of TAPVC: risk factors for adverse outcome. *Eur J Cardiothorac Surg*. 2003;24:28-36.
5. Hickey EJ, Caldarone CA. Surgical management of post-repair pulmonary vein stenosis. *Semin Thorac Cardiovasc Surg Pediatr Card Surg Annu*. 2011;14:101-8.
6. Balasubramanian S, Marshall AC, Gauvreau K, Peng LF, Nugent AW, Lock JE, et al. Outcomes after stent implantation for the treatment of congenital and postoperative pulmonary vein stenosis in children. *Circ Cardiovasc Interv*. 2012;5:109-17.
7. Bando K, Turrentine MW, Ensing GJ, Sun K, Sharp TG, Sekine Y, et al. Surgical management of total anomalous pulmonary venous connection. Thirty-year trends. *Circulation*. 1996;94:Ii12-6.
8. Caldarone CA, Najm HK, Kadletz M, Smallhorn JF, Freedom RM, Williams WG, et al. Relentless pulmonary vein stenosis after repair of total anomalous pulmonary venous drainage. *Ann Thorac Surg*. 1998;66:1514-20.
9. Kato H, Fu YY, Zhu J, Wang L, Aafaqi S, Rahkonen O, et al. Pulmonary vein stenosis and the pathophysiology of "upstream" pulmonary veins. *J Thorac Cardiovasc Surg*. 2014;148:245-53.
10. LaBourene JI, Coles JG, Johnson DJ, Mehra A, Keeley FW, Rabinovitch M. Alterations in elastin and collagen related to the mechanism of progressive pulmonary venous obstruction in a piglet model. A hemodynamic, ultrastructural, and biochemical study. *Circ Res*. 1990;66:438-56.
11. Zhu J, Ide H, Fu YY, Teichert AM, Kato H, Weisel RD, et al. Losartan ameliorates "upstream" pulmonary vein vasculopathy in a piglet model of pulmonary vein stenosis. *J Thorac Cardiovasc Surg*. 2014;148:2550-7.
12. Kawatsu S, Oda K, Saiki Y, Tabata Y, Tabayashi K. External application of rapamycin-eluting film at anastomotic sites inhibits neointimal hyperplasia in a canine model. *Ann Thorac Surg*. 2007;84:560-7.
13. Suzuki T, Saiki Y, Horii A, Fukushige S, Kawamoto S, Adachi O, et al. Atrial natriuretic peptide induces peroxisome proliferator activated receptor gamma during cardiac ischemia-reperfusion in swine heart. *Gen Thorac Cardiovasc Surg*. 2017;65:85-95.
14. van Son JA, Danielson GK, Puga FJ, Edwards WD, Driscoll DJ. Repair of congenital and acquired pulmonary vein stenosis. *Ann Thorac Surg*. 1995;60:144-50.
15. Sadr IM, Tan PE, Kieran MW, Jenkins KJ. Mechanism of pulmonary vein stenosis in infants with normally connected veins. *Am J Cardiol*. 2000;86:577-9, a510.
16. Wilson WR Jr, Ilbawi MN, DeLeon SY, Quinones JA, Arcilla RA, Sulayman RF, et al. Technical modifications for improved results in total anomalous pulmonary venous drainage. *J Thorac Cardiovasc Surg*. 1992;103:861-70.
17. Yoshimura N, Fukahara K, Yamashita A, Doi T, Takeuchi K, Yamashita S, et al. Surgery for total anomalous pulmonary venous connection: primary sutureless repair vs. conventional repair. *Gen Thorac Cardiovasc Surg*. 2017;65:245-51.
18. Hawkins JA, Minich LL, Tani LY, Ruttenberg HD, Sturtevant JE, McGough EC. Absorbable polydioxanone suture and results in total anomalous pulmonary venous connection. *Ann Thorac Surg*. 1995;60:55-9.
19. Douglas YL, Jongbloed MR, den Hartog WC, Bartelings MM, Bogers AJ, Ebels T, et al. Pulmonary vein and atrial wall pathology in human total anomalous pulmonary venous connection. *Int J Cardiol*. 2009;134:302-12.
20. Zohlnhofer D, Nuhrenberg TG, Neumann FJ, Richter T, May AE, Schmidt R, et al. Rapamycin effects transcriptional programs in smooth muscle cells controlling proliferative and inflammatory properties. *Mol Pharmacol*. 2004;65:880-9.
21. Kurdi A, De Meyer GR, Martinet W. Potential therapeutic effects of mTOR inhibition in atherosclerosis. *Br J Clin Pharmacol*. 2016;82:1267-79.
22. Goncharova EA. mTOR and vascular remodeling in lung diseases: current challenges and therapeutic prospects. *FASEB J*. 2013;27:1796-807.
23. Li P, Li YL, Li ZY, Wu YN, Zhang CC, A X, et al. Cross talk between vascular smooth muscle cells and monocytes through interleukin-1beta/interleukin-18 signaling promotes vein graft thickening. *Arterioscler Thromb Vasc Biol*. 2014;34:2001-11.
24. Riedlinger WF, Juraszek AL, Jenkins KJ, Nugent AW, Balasubramanian S, Calicchio ML, et al. Pulmonary vein stenosis: expression of receptor tyrosine kinases by lesional cells. *Cardiovasc Pathol*. 2006;15:91-9.
25. Frangogiannis NG, Michael LH, Entman ML. Myofibroblasts in reperfused myocardial infarcts express the embryonic form of smooth muscle myosin heavy chain (SMemb). *Cardiovasc Res*. 2000;48:89-100.
26. Dancey J. mTOR signaling and drug development in cancer. *Nat Rev Clin Oncol*. 2010;7:209-19.
27. Sousa JE, Costa MA, Abizaid A, Abizaid AS, Feres F, Pinto IM, et al. Lack of neointimal proliferation after implantation of sirolimus-coated stents in human coronary arteries: a quantitative coronary angiography and three-dimensional intravascular ultrasound study. *Circulation*. 2001;103:192-5.
28. Morice MC, Serruys PW, Sousa JE, Fajadet J, Ban Hayashi E, Perin M, et al. A randomized comparison of a sirolimus-eluting stent with a standard stent for coronary revascularization. *N Engl J Med*. 2002;346:1773-80.
29. Laplante M, Sabatini DM. mTOR signaling at a glance. *J Cell Sci*. 2009;122:3589-94.
30. Dutcher JP. Mammalian target of rapamycin inhibition. *Clin Cancer Res*. 2004;10:6382s-7s.
31. Hu JJ, Ambrus A, Fossum TW, Miller MW, Humphrey JD, Wilson E. Time courses of growth and remodeling of porcine aortic media during hypertension: a quantitative immunohistochemical examination. *J Histochem Cytochem*. 2008;56:359-70.
32. Patterson C, Mapera S, Li HH, Madamanchi N, Hilliard E, Lineberger R, et al. Comparative effects of paclitaxel and rapamycin on smooth muscle migration and survival: role of AKT-dependent signaling. *Arterioscler Thromb Vasc Biol*. 2006;26:1473-80.
33. Wang Q, Wan L, Liu L, Liu J. Role of the motor signalling pathway in experimental rabbit vein grafts. *Heart Lung Circ*. 2016;25:1124-32.

Key Words: total anomalous pulmonary vein connection, pulmonary vein stenosis, intimal hyperplasia, rapamycin, smooth muscle cell

APPENDIX E1. DETAILED METHODS

Surgical Procedure

After anesthetic induction with intramuscular injection of medetomidine hydrochloride (0.06 mg/kg) and midazolam (0.3 mg/kg), endotracheal intubation was performed. Intraoperative anesthesia was maintained by inhalation of sevoflurane (1.5%-2.5%). Arterial blood pressure, heart rate, pulmonary arterial pressure, pulmonary capillary wedge pressure, central venous pressure, and cardiac output were monitored through a cervical arterial line and Swan-Ganz catheter inserted from the jugular vein. The body surface area (in meters^2) was calculated using the formula[E1] 0.0734 $\times$ (body weigh)$^{0.656}$, and estimated cardiac index was calculated as normalized cardiac output to body surface area.

Pigs were placed in the right decubitus position for a left fifth intercostal thoracotomy. The left lower pulmonary vein (PV) was dissected free of adhering pleura at the left atrial junction. After heparinization (300 U/kg) and intravenous injection of methylprednisolone (125 mg), the left pulmonary artery was selectively occluded using a Swan-Ganz catheter, and the left lower PV was clamped. The PV was transected subcircumferentially, and the edges were reanastomosed with 7–0 Prolene (Ethicon, Somerville, NJ) running suture (Figure 1, *A* and *B*). Clamp time was 24.7 $\pm$ 5.8 minutes, and the postanastomosed diameter was 72.4% $\pm$ 4.3% of the preanastomosed diameter. The sham group underwent identical procedures, including the similar dissection and clamp (20-25 minutes) of the left lower PV, except for cut and anastomosis of the PV.

An overview of the protocols is shown in Figure 2. We evaluated the model validity in experiment I and the effectiveness of rapamycin film treatment in experiment II. In the acute phase model (1 week model, pulmonary vein obstruction [PVO]: n = 5, and sham: n = 5), pigs underwent hemodynamic assessment and tissue harvest at 1 week postsurgery. The left lung was immediately removed after sacrifice and the pulmonary veins were divided into three segments (Figure E3). The most proximal segment centered 2 cm around the anastomotic site was termed anastomotic PV, and used for histology evaluation. The remained peripheral PV was termed upstream PV, and the midsegment 1-3 cm from the anastomotic site was used for protein assay and the most peripheral segment 3-6 cm from the anastomotic site for histology evaluation.

In the chronic phase model (8 weeks model), 2 PVO pigs underwent tissue harvest at 8 weeks after the procedure, whereas another 9 (PVO: n = 5, sham: n = 4) were subjected to weekly hemodynamic assessment and pulmonary arterial angiography for the evaluation of anastomosed PV patency. These weekly examinations were continued until the anastomosed PV was occluded as evidenced by digital subtraction angiography. Briefly, we occluded the left pulmonary artery using a Swan-Ganz catheter and injected 5 mL iopamidol tracer. When iopamidol was not washed out from the pulmonary artery or the PV could not be visualized in 5 seconds, the PV was considered occluded. These pigs were sacrificed at 4 weeks (PVO: n = 2) or 8 weeks (PVO: n = 3, sham: n = 4) after the procedure, and the left lung harvested for histology evaluation of anastomotic PV and upstream PV segments.

Preparation of Rapamycin-Eluting Film and Treatment

Another 15 pigs were allotted for the rapamycin film treatment study (Figure 2). The preparation of rapamycin-eluting films was described in our previous study,[E2] and several procedures were modified in this study. We selected polylactide-co-glycolide (PLGA) as the biodegradable polymer and based the lower drug concentration on a clinically available rapamycin-eluting stent (140 μg rapamycin in 1 cm^2 stent area).[E3] We dissolved 230 mg PLGA in 5.5 mL chloroform and poured the mixture into a 60-mm diameter polytetrafluoroethylene laboratory dish. To achieve a drug concentration equivalent to the rapamycin-eluting stent, we added 4500 μg rapamycin to the solution and the mixture was stirred for 15 minutes at room temperature. The dish was kept in a fume hood for 1 hour to evaporate the solvent and then vacuum dried for 24 hours at 4°C. The film was peeled off from the dish and cut into 1 cm^2 segments for the in vitro release assays. For the in vivo release assay and evaluation of treatment efficacy, we made 2 $\times$ 3 cm strips to encircle the vascular anastomotic site externally. For preparation, we dissolved 50 mg PLGA in 1.2 mL chloroform and poured the mixture into 2 $\times$ 3 cm dishes under sterile conditions. We tested 2 different doses of rapamycin to examine the dose-response relationship, 1 mg low-dose rapamycin film and 10 mg high-dose rapamycin film. The concentration of rapamycin in the low-dose rapamycin film was nearly equivalent to that of the rapamycin-eluting stent. The same drying process was used for preparation of the in vivo films.

To first evaluate the rapamycin release kinetics from films in vitro, a 1 cm^2 film was incubated in 1 mL phosphate buffered saline buffer as the release medium at 37°C. The release medium was exchanged for fresh medium every day. On days 0, 1, 3, 6, 12, 20, and 28, the film was removed from the medium (n = 3 in each time point) and the remaining rapamycin extracted by soaking the film in 1 mL methanol, followed by measurement of methanol rapamycin concentration using high-performance liquid chromatography (HPLC). HPLC measurement conditions were as follows: mobile phase, acetonitrile/methanol/water (45/40/15 vol%); flow rate, 1.2 mL/min; detection wavelength of 278 nm. The rapamycin retention time was about 7 minutes.

Evaluation of in vivo rapamycin release kinetics was conducted as described in a previous report.[E4] Briefly, we applied the film around pig cervical veins. The cervical veins, including the peripheral tissue were removed 1, 2, 3, or 4 weeks after administration of the films (n = 3 pigs for each time point), cut into small pieces, and homogenized in 1 mL methanol using an ultrasonic homogenizer. Drug from each tissue sample was extracted at 37°C for 24 hours. The samples were centrifuged at 14,000 rpm for 10 minutes and analyzed by HPLC as described above.

Histological Analysis

Paraffin-embedded tissues were sectioned and stained with hematoxylin and eosin. Elastica-Masson staining was performed to quantify intimal hyperplasia in every segment. CellSens Standard software (Olympus, Tokyo, Japan) was used for quantification. The intimal area was measured between the endothelial layer and internal elastic lamina, and the medial area was quantified between the internal elastic lamina and the outside border of smooth muscle cells. The circumference of the internal lamina was used to calculate the radius of the vessel and the extent of intimal hyperplasia is described using intimal area/radius^2 (IA/R^2). This normalizes the measured intimal area to the square of the calculated radius and represents the ratio of the intimal area to an idealized vessel internal luminal area.[E5] In addition, intima-media area/radius^2 (MA/R^2) was used as a measure of normalized intimamedia area to evaluate the extent of medial hypertrophy.[E5] Intimal hyperplasia and medial hypertrophy were assessed at 5 or more radial points in each PV specimen.

Immunohistochemistry

Immunohistochemistry was conducted on other adjacent sections. For single antibody staining, sections were deparaffinized, rehydrated, and subjected to antigen retrieval using sodium citrate buffer. Endogenous peroxidase activity was eliminated by incubation with 0.3% hydrogen peroxide for 30 minutes, and sections were then immersed in blocking buffer for 30 minutes. Sections were incubated overnight at 4°C with a primary antibody against CD31(1:200) (catalog No. 28364; Abcam, Cambridge, United Kingdom; alpha-smooth muscle actin (αSMA) (1:300) (catalog No. 5694; Abcam), nonmuscle myosin heavy chain (SMemb) (1:3000) (catalog No. 7602; Yamasa, Japan), h-caldesmon (1:100) (catalog No. 3576; Merck Millipore, Darmstadt, Germany), calponin (1:100) (catalog No. 3556; Dako, Glostrup, Denmark), Ki-67 (1:100) (catalog No. 7240; Dako), or phospho-mammalian target of rapamycin (phospho-mTOR) (Ser2448) (1:100) (catalog No. 2971; Cell signaling Technology, Danvers, Mass). Biotin-conjugated secondary antibodies were applied for 1 hour at room temperature and then the sections were incubated for 15 minutes with peroxidase-conjugated streptavidin. Subsequently, the sections were developed using 3,3-diaminobenzidine solution (0.5 mg/mL) in the presence of 0.1% hydrogen peroxide. After washing in distilled water, the sections were counterstained with hematoxylin.

For double-immunostaining with αSMA and phospho-mTOR, sections were deparaffinized, immersed in blocking buffer for 30 minutes and then incubated with a 1:300 diluted anti-αSMA antibody for 2 hours at room temperature. To eliminate endogenous peroxidase activity, sections were then incubated with 0.3% hydrogen peroxide for 30 minutes. Biotin-conjugated anti-mouse immunoglobulin antibodies were applied for 20 minutes and sections then incubated for 20 minutes in alkaline phosphatase-labeling streptavidin. Subsequently, the sections were developed using Vector red alkaline phosphatase substrate (Vector laboratories, Burlingame, Calif). Next, sections were treated with sodium citrate buffer for antigen retrieval and incubated with a 1:100 diluted anti-phospho-mTOR antibody overnight at 4°C. Biotin-conjugated antirabbit immunoglobulin antibody was applied for 30 minutes and then the sections were incubated for 15 minutes with peroxidase-conjugated streptavidin. Subsequently, they were developed using HistoGreen (Linaris, Werheim, Germany). For αSMA/Ki-67 double staining, αSMA stain was performed as above, followed by antigen retrieval using antigen retrieval buffer (Nichirei Bioscience, Tokyo, Japan) and incubation with a 1:100 diluted anti-Ki-67 antibody overnight at 4°C. Immunolabeling was then visualized using a horseradish peroxidase-labeled polymer, EnVision + System (Dako), and reacted with HistoGreen.

The Ki-67-positive cells and phospho-mTOR-positive cells in the neointimal area were counted in 5 different fields (40× objective) using the color deconvolution plug-in for ImageJ (National Institutes of Health, Bethesda, Md).

Western Blot Analysis

Western blotting was performed as described previously.[E6,E7] Upstream PV segments 1-3 cm from the anastomotic site were homogenized in lysis buffer and centrifuged to obtain the soluble protein. The protein solution was diluted to half by mixing with sodium dodecyl sulfate–polyacrylamide gel electrophoresis buffer and β-mercapthoethanol, boiled for 5 minutes, electrophoresed on 5% to 20% sodium dodecyl sulfate-polyacrylamide gels (Wako, Tokyo, Japan), and blotted onto polyvinylidene difluoride membranes (Atto, Tokyo, Japan). The blots were then probed with a 1:3000 diluted anti-nonmuscle myosin heavy chain (catalog No. 7602; Yamasa), 1:1000 diluted anti-calponin (catalog No. 3556; Dako), 1:1000 anti-mTOR (catalog No. 2983; Cell

Signaling), 1:500 diluted anti-phospho-mTOR (Ser2448) (catalog No. 2971; Cell Signaling), 1:1000 diluted anti-4E-BP1 antibody (catalog No. 9452; Cell Signaling), or 1:500 diluted anti-phospho-4E-BP1 (Ser65) antibody (catalog No. 9451; Cell Signaling). A 1:1000 diluted anti-glyceraldehyde-3-phosphate dehydrogenase antibody (catalog No. 2118; Cell Signaling) was used as the gel loading control A sheep antimouse horseradish peroxidase-conjugated immunoglobulin antibody or the donkey antirabbit horseradish peroxidase-conjugated immunoglobulin antibody (GE Healthcare UK Limited, Buckinghamshire, United Kingdom) was as the secondary antibody at 1:3000. The blot was visualized with enhanced chemiluminescence detection (Amersham International PLC, Little Chalfont, United Kingdom). Chemiluminescence was measured using image Quant LAS7000 (GE Healthcare Bio-Sciences AB, Bjorkgatan, Sweden).

E-References

E1. Kelley KW, Curtis SE, Marzan GT, Karara HM, Anderson CR. Body surface area of female swine. *J Anim Sci*. 1973;36:927-30.

E2. Kawatsu S, Oda K, Saiki Y, Tabata Y, Tabayashi K. External application of rapamycin-eluting film at anastomotic sites inhibits neointimal hyperplasia in a canine model. *Ann Thorac Surg*. 2007;84:560-7.

E3. Morice MC, Serruys PW, Sousa JE, Fajadet J, Ban Hayashi E, Perin M, et al. A randomized comparison of a sirolimus-eluting stent with a standard stent for coronary revascularization. *N Engl J Med*. 2002;346:1773-80.

E4. Reddy MK, Vasir JK, Sahoo SK, Jain TK, Yallapu MM, Labhasetwar V. Inhibition of apoptosis through localized delivery of rapamycin-loaded nanoparticles prevented neointimal hyperplasia and reendothelialized injured artery. *Circ Cardiovasc Interv*. 2008;1:209-16.

E5. Zhu J, Ide H, Fu YY, Teichert AM, Kato H, Weisel RD, et al. Losartan ameliorates "upstream" pulmonary vein vasculopathy in a piglet model of pulmonary vein stenosis. *J Thorac Cardiovasc Surg*. 2014;148:2550-7.

E6. Kondo E, Horii A, Fukushige S. The human PMS2L proteins do not interact with hMLH1, a major DNA mismatch repair protein. *J Biochem*. 1999;125:818-25.

E7. Suzuki T, Saiki Y, Horii A, Fukushige S, Kawamoto S, Adachi O, et al. Atrial natriuretic peptide induces peroxisome proliferator activated receptor gamma during cardiac ischemia-reperfusion in swine heart. *Gen Thorac Cardiovasc Surg*. 2017;65:85-95.

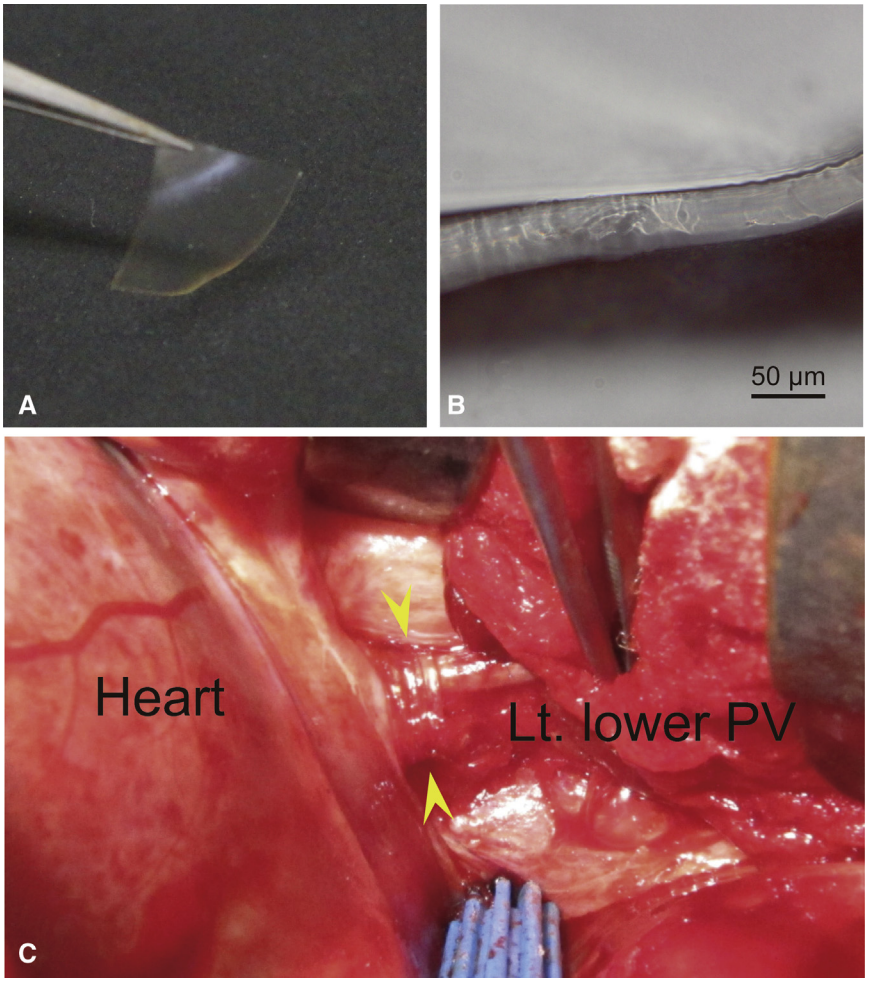

FIGURE E1. The appearance of the rapamycin-eluting film. A, The film was transparent and flexible. B, Microscopic observation revealed that films were approximately 45 μm thick, and therefore suitable for external application at the vascular anastomotic site. C, A depiction of external application at the anastomotic site (*arrowhead indicates the film*). *PV*, Pulmonary vein.

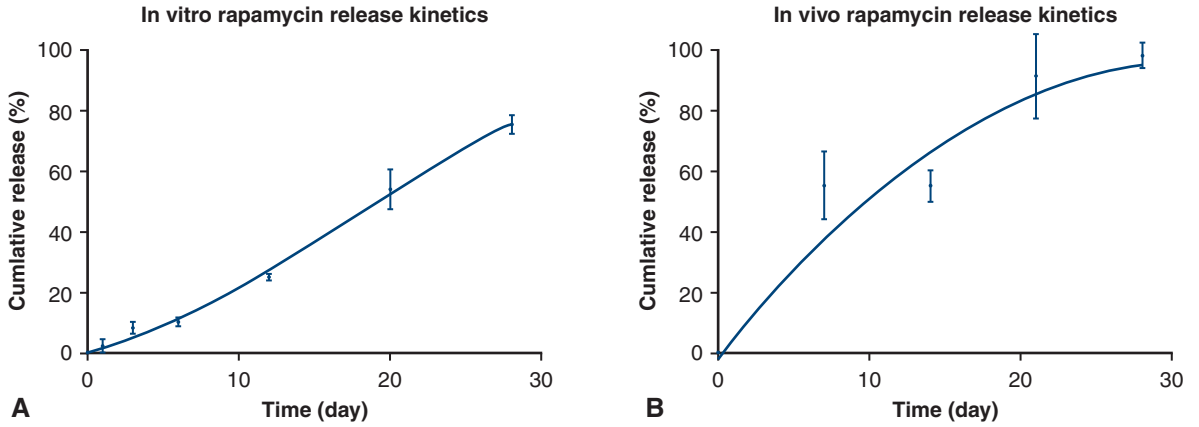

FIGURE E2. In vitro and vivo cumulative release profile of rapamycin from the film. A, In vitro release kinetics were estimated by high performance liquid chromatography. Cumulative release of rapamycin was about 10% after 1 week and 80% after 1 month in vitro. B, In vivo cumulative rapamycin release measurements indicated that approximately 50% was released after 1 week and 100% after 1 month, substantially faster than in vitro.

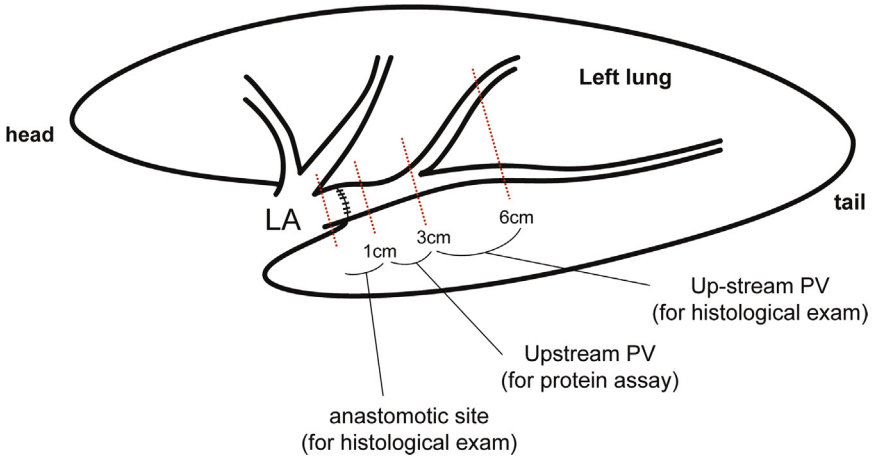

FIGURE E3. Sectioning of resected pulmonary veins. The pulmonary veins (*PVs*) were divided 3 segments. The proximal segment, including the anastomosis, was called the anastomotic site, and the other 2 segments were called the upstream site. The anastomotic site and the distal upstream PV segments were used for histological analysis and the middle upstream PV segment for Western blot analysis. *LA*, Left atrium.

TABLE E1. Diameter of the left lower pulmonary vein

	1 wk model			8 wk model				
Diameter	**PVO (n = 5)**	**H-RAP (n = 5)**	***P* value**	**Sham (n = 4)**	**PVO (n = 7)**	**L-RAP (n = 5)**	**H-RAP (n = 5)**	***P* value**
Preoperative (mm)	9.0 (8.5-10.5)	9.5 (8.5-10.0)	.66	9.5 (9.0-10.0)	9.0 (7.5-12.0)	10.0 (8.0-10.5)	9.0 (8.0-10.0)	.42
Postoperative (mm)	6.5 (6.0-7.5)	6.5 (5.5-7.0)	.74	9.5 (9.0-10.0)	6.5 (5.5-9.0)	7.5 (6.0-8.0)	6.5 (5.5-8.5)	.02*
Post/pre (%)	71 (67-78)	68 (65-74)	.25	100 (100-100)	73 (67-80)	80 (57-93)	72 (68-85)	.01*

Values are presented as median (range). *PVO*, Pulmonary vein obstruction; *H-RAP*, high-dose rapamycin film; *L-RAP*, low-dose rapamycin film; *Post*, postoperative; *Pre*, preoperative. *There was no significant difference among PVO, L-RAP, and H-RAP.